Sulfidic patch formation by macroalgal blooms impairs seagrass photosynthesis in the Gulf of Aqaba, Red Sea

Neta Soto
Ben-Gurion University of the Negev
Maayan Mazal Malul
Ben-Gurion University of the Negev
Gilad Antler
giladantler@gmail.com

Ben-Gurion University of the Negev

Research Article

Keywords: Halophila stipulacea, biological sulfate reduction, Gulf of Aqaba, macroalgal bloom, porewater sulfide, cryptic sulfur cycle, seagrass stress, winter convective mixing

Posted Date: June 24th, 2026

DOI: https://doi.org/10.21203/rs.3.rs-9731786/v1

Additional Declarations: No competing interests reported.

Sulfidic patch formation by macroalgal blooms impairs seagrass photosynthesis in the Gulf of Aqaba, Red Sea

Neta Soto[1], Maayan Mazal Malul[2,3], Gilad Antler[4,*]

1. Department of Environmental, Geo-informatics and Urban Planning Sciences, Ben Gurion University, Beer Sheva, Israel
2. Jusidman Science Center for Youth, Ben-Gurion University of the Negev, Beer Sheva, Israel
3. Alpha program, Future Scientists Program, Tel Aviv, Israel
4. Department of Earth and Environmental Sciences, Ben Gurion University, Beer Sheva, Israel

*Corresponding author, email: giladantler@gmail.com

Abstract

Seagrass meadows are among the most productive and ecologically significant coastal ecosystems globally. They are, however, acutely vulnerable to sediment sulfide toxicity generated during periods of organic enrichment. In the oligotrophic Gulf of Aqaba (GoA), the dominant seagrass *Halophila stipulacea* is exposed to an annual macroalgal bloom triggered by deep winter convective mixing, yet the biogeochemical consequences for meadow integrity remain uninvestigated. We document a biogeochemical cascade linking winter nutrient injection to sulfidic stress in *H. stipulacea* meadows at North Beach, Eilat. Porewater sulfide, total alkalinity (TA), dissolved inorganic carbon (DIC), and dissolved oxygen were measured beneath decomposing macroalgal mats and adjacent algae-free sediments at bloom onset (March 2024) and senescence (May 2024). Sulfide beneath mats increased by approximately two orders of magnitude during senescence, reaching a maximum of 3.6 mM, while algae-free sediments remained near baseline (<0.014 mM). Co-elevation of TA and DIC beneath mats is consistent with active biological sulfate reduction. Dissolved oxygen at the sediment-water interface was near zero throughout a 48-hour deployment in May, compared to partial diel recovery in March. A mesocosm experiment established the first dose-response relationship for *H. stipulacea*, with

photosynthesis declining progressively with increasing sulfide and becoming negative above approximately 3 mM. Anaerobic slurry experiments demonstrate that macroalgal organic matter generates sulfide within a few days. Overall, these results demonstrate that bloom-driven organic loading overwhelms the GoA sediment iron-buffering system, generating sulfidic microenvironments that impair *H. stipulacea* photosynthesis and threaten meadow integrity on a predictable annual cycle.

Keywords: *Halophila stipulacea*; biological sulfate reduction; Gulf of Aqaba; macroalgal bloom; porewater sulfide; cryptic sulfur cycle; seagrass stress; winter convective mixing

1. Introduction

Seagrass meadows are among the most productive coastal ecosystems on Earth, supporting biodiversity, nutrient cycling, and long-term carbon burial [1, 2]. Despite their ecological and geochemical importance, seagrass meadows are in global decline, with losses accelerating over the past several decades due to coastal eutrophication, light reduction, and thermal stress [3]. Among the proximate causes of seagrass mortality, sulfide toxicity has emerged as one of the most pervasive and mechanistically well characterized [4-8]. Hydrogen sulfide (H_2S), the gaseous form of dissolved sulfide, is produced by microbial sulfate reduction in anoxic environments, intrudes plant tissues, and inhibits cytochrome c oxidase at concentrations as low as 1 to 10 μM, blocking aerobic respiration in belowground tissues [9, 10]. Throughout this study, “sulfide” refers to total dissolved sulfide ($\Sigma H_2S = H_2S + HS^- + S^{2-}$); the term H_2S is used only where the specific gaseous species is intended. Seagrasses normally protect themselves through radial oxygen loss (ROL) from roots, which maintains an oxic microzone in the rhizosphere that chemically excludes sulfide [11]. Under low-light or hypoxic conditions, however, this oxic microshield collapses, allowing gaseous H_2S to intrude through root aerenchyma into meristematic tissue and triggering mortality [12, 13].

The Gulf of Aqaba (GoA) is a naturally oligotrophic, semi-enclosed basin at the northern tip of the Red Sea, where surface waters are nutrient depleted year-round but undergo a single annual deep convective mixing event each winter [14, 15]. This convective cycle

erodes the nitracline and raises surface nitrate concentrations from near zero (<0.1 μM in summer) to approximately 0.6 μM, fueling a phytoplankton and macroalgal bloomthat peaks at restratification in late winter to early spring [16,18-19]. Bloom intensity and duration scale with mixing depth: in deep-mixing years, when the mixed layer reaches 700 m or deeper, sustained phytoplankton and benthic macroalgal blooms persist from late winter through May, whereas in shallow-mixing years (~300 m) blooms are weaker and shorter [19, 20]. Anomalously deep mixing events have also been associated with coral mortality along the GoA reef margin, underscoring that the convective cycle can drive acute ecological disturbance beyond the phytoplankton and algal bloom response [18]. Benthic macroalgal blooms in the GoA are dominated by ephemeral filamentous and foliose taxa that proliferate over soft-sediment habitats, including seagrass meadows, and senesce in late spring as restratification reestablishes oligotrophic conditions in the photic zone [18, 20]. The decomposing biomass settles onto the underlying sediment, delivering a concentrated pulse of labile organic matter to a system otherwise characterized by low organic loading. Under undisturbed conditions, GoA sediment geochemistry buffers against free sulfide accumulation through a tightly coupled cryptic sulfur cycle [21]. A pulse of labile macroalgal organic matter can, however, overwhelm this buffering capacity by driving sulfate reduction faster than reactive iron can be replenished, as demonstrated in analogous systems where bloom-driven organic loading depletes the reactive Fe pool within days [22].

The dominant seagrass of the northern GoA is *Halophila stipulacea (H. stipulacea)*, a small tropical species native to the Red Sea, Arabian Gulf, and western Indian Ocean [23]. It forms monospecific meadows covering approximately 707,000 m^2 across a depth range of 1 to 50 m along the Eilat coastline [24, 25]. This species is small-bodied, with leaves typically 4 to 6 cm long and thin rhizomes that sit at or near the sediment surface, and it produces approximately one new shoot every 5.9 days with rhizome elongation rates near 0.2 cm d^{-1} [26]. Above-ground biomass, shoot density, and percent cover at the Eilat North Beach site exhibit a clear seasonal cycle, increasing by approximately 18% in biomass and 35% in shoot density between February and July [27, 28]. This species is also broadly recognized as one of the most stress-tolerant seagrasses globally, acclimating across more than a 20-fold light gradient within one week and tolerating

temperatures from approximately 11 to 38°C and salinities from 25 to 60 ppt [23]. Despite this physiological breadth, *H. stipulacea* exhibits the highest sulfide intrusion rates of any Mediterranean seagrass studied, with stable sulfur isotope analyses indicating that 30 to 50% of tissue sulfur derives from sedimentary sulfide even where porewater concentrations are undetectable [29]. This disproportionate vulnerability traces to the species' small stature and minimal belowground biomass, which constrain the ROL capacity that larger seagrasses use to maintain a sulfide-excluding rhizospheric microzone. However, no direct ROL measurements have been published for *H. stipulacea*, and no controlled sulfide dose-response experiments have been conducted on this species. Moreover, no seasonal porewater sulfide baseline exists for any healthy GoA seagrass meadow, representing a critical gap in understanding susceptibility to bloom-driven sulfidic stress [21, 31-32].

In this study, we document a biogeochemical cascade linking annual deep winter convective mixing in the GoA through *in situ* macroalgal bloom dynamics to sulfidic stress on *H. stipulacea* meadows at North Beach, Eilat. Porewater and overlying-water chemistry (total dissolved sulfide, total alkalinity (TA), dissolved inorganic carbon (DIC)) and oxygen dynamics were measured at bloom onset (March 2024) and bloom senescence (May 2024), beneath a seagrass meadow covered by algal mats and in adjacent algae-free meadow. Additionally, a controlled sulfide addition mesocosm experiment was used to examine the threshold of dose-response porewater sulfide concentration and *H. stipulacea* photosynthetic performance. Anaerobic slurry decomposition incubations were conducted to characterize the relative capacity of macroalgal versus seagrass tissue fractions to drive sulfide production in GoA sediments. Here, we combine seasonal porewater chemistry under macroalgal mats and algae-free meadows with a controlled sulfide exposure experiment on *H. stipulacea*. This design resolves whether bloom decomposition generates porewater sulfide above the iron-buffered GoA baseline, how the signal evolves from bloom onset to senescence, and at what concentration sulfide begins to impair photosynthesis under native conditions.

2. Materials and Methods

2.1 Study site

Field work was conducted at North Beach, Eilat, GoA, Israel (29°33′N, 34°57′E; Fig. 1A). The GoA is a narrow (14 to 26 km), deep (maximum ~1,850 m at the Aragonese Deep) basin separated from the Red Sea by a sill at the Straits of Tiran (~250 to 270 m) that blocks cold deep-water exchange, producing weak stratification that is readily eroded by winter surface cooling. Mixed layer depths in winter typically reach 300 to 700 m and exceed the 730 m floor of the open-sea monitoring station (Station A) in 2022 [20]. Sea surface temperature at the IUI pier follows a regular seasonal cycle, with a multi-decadal climatological minimum of approximately 21.4°C in February and a maximum near 27°C in August, on a long-term warming trend of ~0.36 to 0.49°C per decade since 1988 [20]. Coastal salinity is stable at 40.2 to 41.2‰ year-round [20]. Surface chlorophyll-a tracks the convective cycle, with the multi-annual climatological maximum (~0.5 mg m^{-3}) in March, declining to a summer minimum (<0.2 mg m^{-3}) under stratified, oligotrophic conditions [20; Fig. 1]. Bloom intensity scales with mixing depth: deep-mixing winters (e.g., 2012, 2022) produce sustained phytoplankton and benthic algal blooms extending into May, whereas shallow-mixing years yield weaker, shorter-lived blooms [20].

The North Beach site supports a shallow (2 to 6 m depth) *H. stipulacea* meadow on fine-grained, organically enriched carbonate sediment, located along an anthropogenically influenced coastal segment with a documented history of aquaculture and urban runoff [25, 27, 32]. The site supports the largest continuous H. stipulacea meadow on the Israeli coast, with above-ground biomass and shoot density exceeding those at the less impacted South Beach site within the Eilat Marine Reserve [27, 28]. NMP coastal monitoring records irregularly elevated nutrient concentrations at the northern stations in recent years, attributed in part to terrestrial inputs from the Kinet Canal [20]. Bloom senescence in late spring generates decomposing macroalgal mats that settle onto the seagrass meadow and adjacent bare sediment. Recurrent black-and-white sulfidic patches are a conspicuous feature of North Beach during this period (Fig. 1), associated with porewater sulfide concentrations exceeding several hundred micromolar in comparable systems [30]. The black coloration reflects iron sulfide mineral precipitation, while the white component is attributable to sulfide-oxidizing bacterial biofilms.

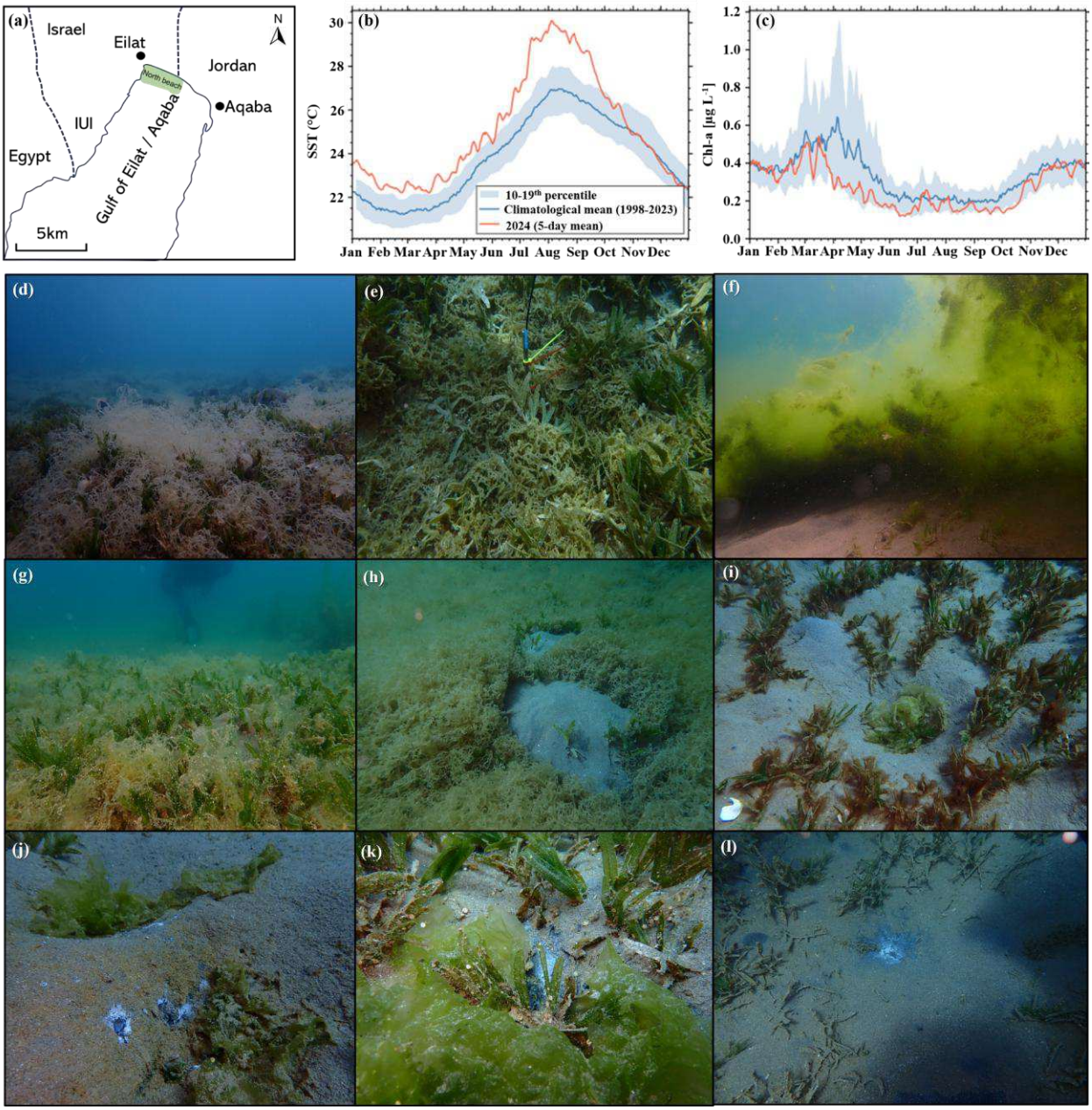

Fig. 1:*(a) Map of the study site at the Gulf of Aqaba, northern Red Sea, with the North Beach monitoring site in blue. Seasonal oceanographic dynamics in the Gulf of Aqaba during 2024 (red line, 5-day mean) relative to the climatological mean for 1998–2023 (blue line) and the 10–19th percentile range (shaded blue): (b) sea surface temperature (SST, °C) and (c) chlorophyll a (Chl-a) concentration (µg L^{-1}). (d-l) underwater*

photographs documenting the temporal progression of the seagrass meadow, algae at North Beach.

2.2 Field sampling

Porewater and water-column samples were collected on two occasions representing contrasting bloom stages, bloom onset (late March 2024) and bloom senescence (late May 2024). At each sampling event, ten replicate porewater samples were extracted from the upper 5 cm of sediment at paired stations beneath intact macroalgal mats overlying seagrass and from adjacent algae-free seagrass meadow. Porewater was extracted *in situ* using Rhizon samplers with 3D-printed depth-constraining sleeves, as described in Dutta et al. (2022) [30]. Samples were collected into pre-evacuated glass vials containing 1 mL of 4% zinc acetate solution to fix dissolved sulfide as zinc sulfide and prevent oxidation. Overlying water samples were collected at each station using 20 mL syringes and immediately filtered through 0.22 µm polyethersulfone filters.

A spatial transect was also established across a single representative sulfidic patch at both sampling events. Porewater and overlying water samples were collected at regular intervals along the transect axis, spanning the interior of the patch, its margin, and the adjacent unvegetated and vegetated sediment. This transect provides a spatial complement to the paired-station comparison and tracks the lateral biogeochemical gradient from patch center to background.

Dissolved oxygen was measured in situ using optical oxygen sensors (optodes, PyroScience GmbH) positioned immediately above the sediment surface below the macroalgal mat and in adjacent algae-free seagrass at each timepoint. Due to logistical constraints, a single sensor deployment was conducted at each station and timepoint. The paired porewater chemistry measurements (n = 10 per station) constitute the primary replicated dataset, and oxygen data are therefore interpreted as indicative rather than statistically replicated.

2.3 Slurry decomposition experiment

To characterize the relative capacity of macroalgal versus seagrass detritus to drive sulfide production in GoA sediments, a closed-system anaerobic slurry incubation experiment was conducted at the IUI Eilat laboratory. Macroalgae (*Ulva lactuca*) and *H. stipulacea* were collected by hand from North Beach (Permit #2023/43223; Israel Nature and Parks Authority). Seagrasses were separated into leaves, and rhizomes and roots. All organic matter fractions were rinsed in deionized water, oven-dried overnight at 60°C and ground to a homogeneous powder, and sieved at 500 µm. Sediment was collected from North Beach by core (15 cm × 5 cm diameter) at 5 m depth on the same sampling day. Seagrasses and belowground structures were removed from cores used as the sediment matrix. The upper 2.5 cm of each core was sliced and mixed with anoxic filtered seawater that had been continuously sparged with N_2 gas to remove dissolved oxygen prior to sediment addition. Organic matter fractions were added individually to separate slurry mixtures at a loading of 0.5 g dry weight per 50 g wet sediment (~1% w/w). Mixtures were dispensed into 15 mL polypropylene tubes or 20 mL glass vials sealed with crimped rubber stoppers to maintain anaerobic headspace. Treatments included macroalgae, seagrass leaves, rhizomes and roots (grouped together as below-ground biomass), and an unamended sediment control. All treatments were run in triplicates, with individual vials sacrificed at sequential timepoints (approximately every 1 to 3 days) over a 25-day incubation. At each timepoint, sacrificed vials were subsampled for TA, DIC, total sulfide (ΣH_2S), sulfate (SO_4^{2-}), ammonium (NH_4^+), and phosphate (PO_4^{3-}).

2.4 Mesocosm sulfide addition experiment

To quantify the photosynthetic response of *H. stipulacea* to porewater sulfide concentrations comparable to those measured in field sulfidic patches, a controlled mesocosm experiment was conducted at IUI Eilat. Living *H. stipulacea* individuals were collected from the North Beach at 5 m depth and transplanted into a 1 m³ tank filled with seawater and sediment from the same site. Plants were acclimated for two weeks under flowing Red Sea seawater maintained at ambient temperature (~24 °C). A localized sulfide patch was generated within the tank by inserting crushed *U. lactuca* biomass into the sediment at the center of the tank, enclosed in a perforated 1.5 mL microcentrifuge tube to create an organic matter hotspot for anaerobic respiration (Fig. 2a). The tank floor

was divided into a 5 × 5 grid (25 cells, ~0.04 m² each), with an additional finer 5 × 5 grid placed over the sulfide source to resolve the steep sulfide gradient near the patch interior. Eleven *H. stipulacea* individuals were distributed at varied distances from the sulfide source. After 7 days, porewater was extracted from each grid cell at ~3 cm depth using Rhizon samplers, with samples fixed in 4% zinc acetate as described above. Porewater sulfide concentrations were mapped across the tank using cubic spline interpolation and assigned to the grid cell position of each plant (Fig. 2b).

Immediately following porewater sampling, each plant was removed and placed individually into a sealed 1 L glass vessel containing filtered seawater. Net photosynthesis was measured as the rate of O_2 accumulation over 30 min under ambient light using a contactless optical oxygen sensor (PyroScience GmbH), calibrated against air-saturated seawater and N_2-sparged seawater reacted with Na_2SO_3. Photosynthetic rate was normalized to total leaf area, determined from digital images of excised leaves analyzed in ImageJ (version 1.54i). Following gas exchange measurements, plants were dissected into leaves (sorted by shoot number), rhizomes, and roots. Each fraction was photographed for area determination, weighed fresh, and weighed again after oven-drying at 60 °C to obtain dry biomass. The aboveground-to-total biomass ratio was calculated as leaf dry mass divided by total plant dry mass.

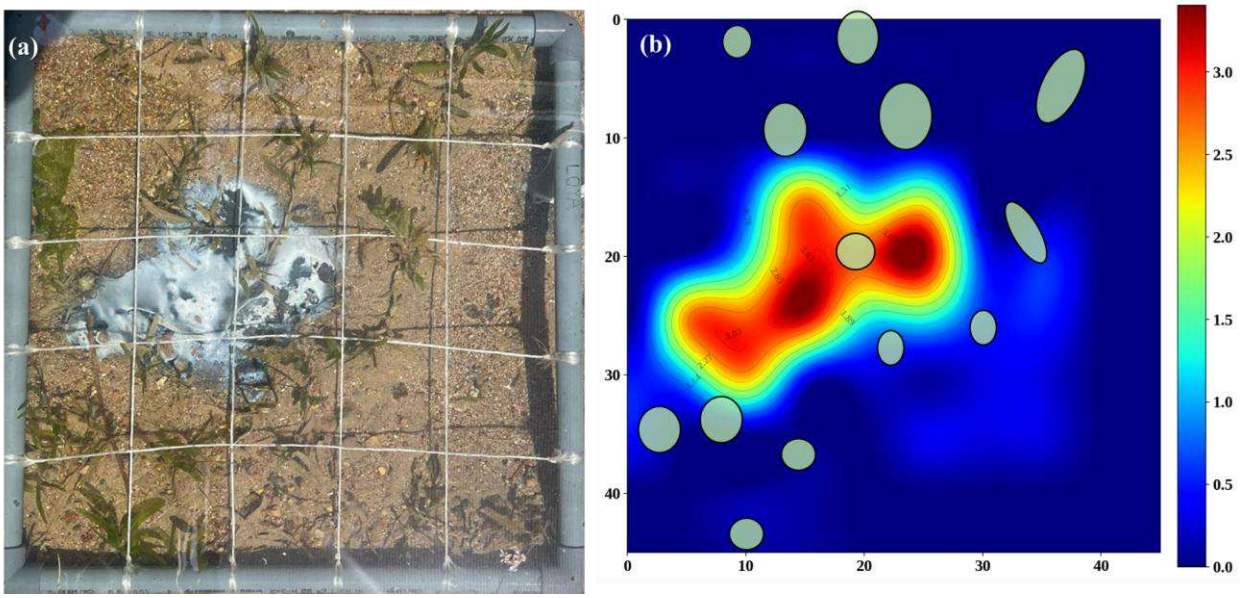

Fig. 2 *Mesocosm setup for the macroalgal decomposition experiment. (a) Photograph of the sediment patch enriched with senescent macroalgal biomass, showing the visible sulfidic (black) sediment surface and the positions of individual H. stipulacea shoots transplanted into the patch. (b) Spatial distribution of total dissolved porewater sulfide (mM) across the same sediment area, sampled on a 5 × 5 cm grid and interpolated using cubic spline smoothing. Light green circles in panel b symbols mark the seagrass positions shown in panel a. Both panels share the same coordinate system (cm).*

2.5 Analytical methods

TA was determined by Gran titration using 0.005 M HCl calibrated against certified reference material [33], performed with a Titroline 7000 automated titrator (SI Analytics)with a precision of ±20 µeq kg^{-1}. DIC was measured using a DIC analyzer (Apollo AS-C6L) calibrated against certified reference material [33], with a precision of ±0.5%. Total dissolved sulfide ($\Sigma H_2S = H_2S + HS^- + S^{2-}$) was quantified by the methylene blue colorimetric method [34], with samples preserved in zinc acetate prior to analysis and absorbance measured at 668 nm by UV-Vis spectrophotometry (Agilent Cary 8454). Sulfide concentrations in porewater samples are reported as total sulfide corrected for dilution by the zinc acetate fixative using gravimetric determination of extracted porewater volume. Phosphate (PO_4^{3-}) was determined by the molybdenum blue colorimetric method at 885 nm [35]. Sulfate was measured by ion chromatography. Ferrous iron was quantified using the ferrozine colorimetric method at 562 nm [36]. Ammonium was determined by fluorescence spectrophotometry (Varian Cary Eclipse) following established protocols.

Statistical analysis

DIC, TA, and dissolved sulfide concentrations were analyzed using linear mixed-effects models (LMMs). Sampling dates (March and May 2024), site type (below algae mat vs. algae mat free), and water compartment (porewater vs. overlying water column) were included as fixed effects, along with all two-way and three-way interaction terms. To

account for the paired sampling design, sampling point identity was included as a random intercept. Sulfide concentrations were log-transformed prior to analysis using log(x + 1) to improve residual normality and homogeneity of variance. Model assumptions were evaluated by inspection of residual histograms, normal Q–Q plots, and residuals-versus-fitted plots. Fixed effects were assessed using Type III Wald χ^2 tests, and pairwise post-hoc comparisons among site × compartment combinations were conducted using estimated marginal means with Tukey-adjusted P-values. All analyses were performed in R version 4.5.1.

3. Results

3.1 Bottom-water oxygen dynamics

Continuous oxygen records above and below the macroalgal mat at North Beach diverged sharply between bloom onset and bloom senescence (Fig. 3). At both timepoints, water-column oxygen above the mat tracked diel cycles of photosynthesis and respiration and remained well above 100µM throughout each deployment. Oxygen at the sediment-water interface was systematically lower than in the overlying water and exhibited progressively greater drawdown as the bloom advanced.

At bloom onset in March 2024, oxygen above the mat ranged from 182 to 277 µM over the 25-hour record. Below-mat oxygen tracked the same diel pattern but at consistently lower concentrations during daylight hours (Fig. 3A). A nocturnal drawdown reduced below-mat oxygen to near-anoxia (<5 µM) for several hours before sunrise, followed by recovery to values approaching those of the overlying water (~230 µM) within hours of dawn.

At bloom senescence in May 2024, the two oxygen records decoupled (Fig. 3B). Oxygen above the mat remained dynamic over the 48-hour deployment, oscillating between 8 and 353 µM in phase with the diel cycle. Below-mat oxygen remained at or near zero (<2 µM) for the full deployment, with two brief excursions to 100 to 135 µM during midday hours on 22 May. Mean below-mat oxygen declined from approximately 130 µM in March to approximately 5 µM in May. The diel recovery of below-mat oxygen that was evident at bloom onset was absent during senescence.

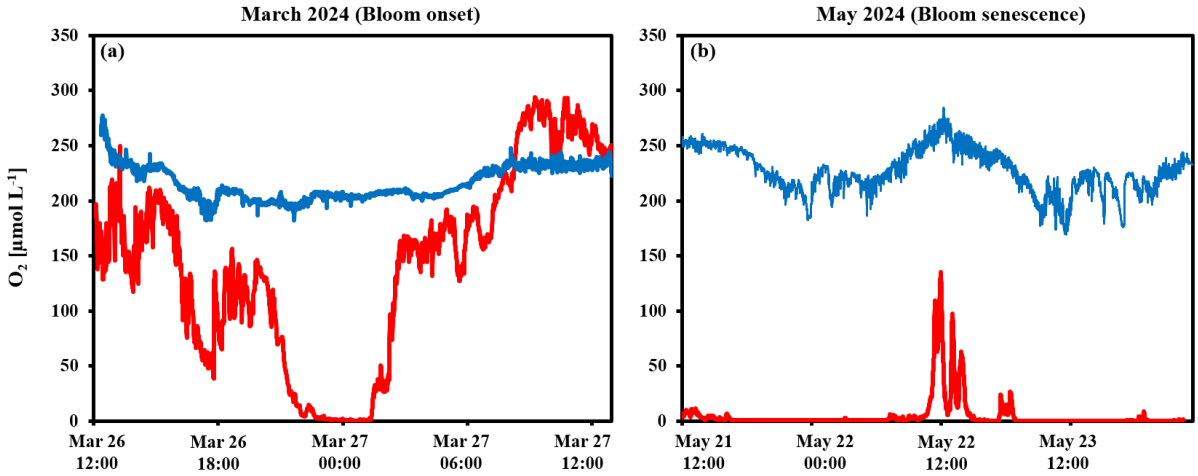

Fig. 3 *Continuous bottom-water oxygen concentrations (µM) recorded by optode sensors above the macroalgal mat (blue) and below the mat at the sediment-water interface (red) at North Beach, Eilat, Gulf of Aqaba, during (a) bloom onset in late March 2024 and (b) bloom senescence in late May 2024.*

3.2 Porewater and water-column geochemistry: paired station comparison

Porewater DIC and TA were elevated beneath macroalgal mats relative to algae-free seagrass sediments at both sampling timepoints (Fig. 4a-d). In March, median porewater DIC was 3.43 mM below mats compared to 2.42 mM in algae-free sediments, and median TA was 3.73 mM below mats compared to 2.59 mM in algae-free sediments. Individual porewater DIC values reached 4.35 mM and TA reached 4.70 mM within the below-mat group. In May, the same pattern held, with median porewater DIC of 2.91 mM below mats versus 2.49 mM in algae-free sediments and median TA of 3.06 mM below mats versus 2.65 mM in algae-free sediments. The upper tail of the below-mat distributions extended further in May, with individual DIC values reaching 4.88 mM and TA reaching 5.01 mM. Water-column DIC and TA were largely invariant across treatments in March (~2.15 mM and ~2.54 mM, respectively). By May, water-column DIC and TA below mats were moderately elevated relative to algae-free areas (median 2.54 versus 2.17 mM for DIC; 2.69 versus 2.50 mM for TA), consistent with partial coupling between porewater efflux and the overlying water column by bloom senescence.

Porewater sulfide showed a pronounced seasonal and spatial contrast (Fig. 4e-f). In March, porewater sulfide was low across both treatments, with medians of 0.013 mM below mats and 0.014 mM in algae-free sediments and no clear separation between the two groups. By May, porewater sulfide beneath mats increased by approximately two orders of magnitude, reaching a median of 1.20 mM and individual values as high as 3.60 mM. Algae-free porewater sulfide remained low in May (median 0.003 mM), comparable to March levels and approaching the sub-micromolar background expected from the GoA's iron-buffered cryptic sulfur cycle [21, 37]. Water-column sulfide below mats reached a median of 0.197 mM in May, while water-column sulfide at algae-free stations remained low (median 0.066 mM). The shift in both porewater and water-column sulfide from March to May was confined to stations beneath decomposing algal mats.

DIC concentrations were significantly affected by sampling date, site type, and water compartment (linear mixed-effects model, Type III Wald χ^2 tests; date: $\chi^2 = 10.63$, $P = 0.001$; site: $\chi^2 = 7.07$, $P = 0.008$; compartment: $\chi^2 = 31.80$, $P < 0.001$). A significant site × compartment interaction was also detected ($\chi^2 = 6.30$, $P = 0.012$), indicating that the magnitude of porewater–overlying water differences depended on the presence of algal mats. Neither the date × compartment interactionnor the three-way interaction were significant ($P = 0.34$ and $P = 0.76$, respectively). Porewater beneath algal mats had the highest DIC concentrations (3280 ± 98 μM), exceeding porewater at unvegetated sites by ~32% (2494 ± 104 μM; $P < 0.001$), overlying water beneath mats by ~34% (2439 ± 98 μM; $P < 0.001$), and overlying water at unvegetated sites (2160 ± 104 μM; $P < 0.001$). Notably, porewater at unvegetated sites did not differ significantly from overlying water beneath mats ($P = 0.98$). At sites lacking algal mats, porewater and overlying water DIC were more similar, though porewater remained slightly but significantly elevated ($P = 0.008$). Together, these results indicate substantial DIC accumulation in porewaters beneath algal mats relative to both unvegetated sediments and overlying waters.

TA was also significantly influenced by sampling date, site type, and water compartment (linear mixed-effects model, Type III Wald χ^2 tests; date: $\chi^2 = 8.25$, $P = 0.004$; site: $\chi^2 = 8.11$, $P = 0.004$; compartment: $\chi^2 = 22.65$, $P < 0.001$). A significant site × compartment interaction was also detected ($\chi^2 = 9.66$, $P = 0.002$), indicating that porewater–overlying

water differences in alkalinity depended on the presence of algal mats. Neither the date × compartment interaction nor the three-way interaction were significant ($P = 0.17$ and $P = 0.57$, respectively). Porewater beneath algal mats had the highest alkalinity (3.5 ± 0.1 meq kg^{-1}), exceeding porewater at unvegetated sites by ~32% (2.6 ± 0.1 meq kg^{-1}; $P < 0.001$), overlying water beneath mats by ~31% (2.7 ± 0.1 meq kg^{-1}; $P < 0.001$), and overlying water at unvegetated sites (2.5 ± 0.1 meq kg^{-1}; $P < 0.001$). At sites lacking algal mats, porewater and overlying water alkalinity differed by only ~5% and did not differ significantly ($P = 0.57$), and no significant differences were detected among any of the remaining unvegetated and overlying-water groups (all $P > 0.57$). These results indicate pronounced alkalinity accumulation in porewaters beneath algal mats relative to both unvegetated sediments and overlying waters.

Log-transformed sulfide concentrations were significantly influenced by sampling date (linear mixed-effects model, Type III Wald χ^2 test; $\chi^2 = 34.24$, $P < 0.001$), while no overall main effects of site type or water compartment were detected ($P > 0.95$ for both). Significant date × compartment ($\chi^2 = 54.07$, $P < 0.001$) and site × compartment interactions ($\chi^2 = 9.00$, $P = 0.003$) were observed, however, indicating that sulfide partitioning between porewater and overlying water varied both temporally and with algal mat presence. The three-way interaction was notsignificant ($P = 0.35$). Compartment-specific sulfide patterns differed markedly between sampling dates. In March 2024, sulfide concentrations did not differ significantly between porewater and overlying water beneath algal mats ($P = 0.95$), whereas porewater at unvegetated sites was approximately 95% higher than overlying water ($P < 0.001$). By May 2024, this pattern had reversed: overlying water sulfide concentrations substantially exceeded porewater at both mat-covered and unvegetated sites (both $P < 0.001$), with the highest values recorded in overlying water beneath algal mats. These results indicate strong temporal shifts in sulfide partitioning between porewaters and overlying waters, particularly in association with algal mat presence.

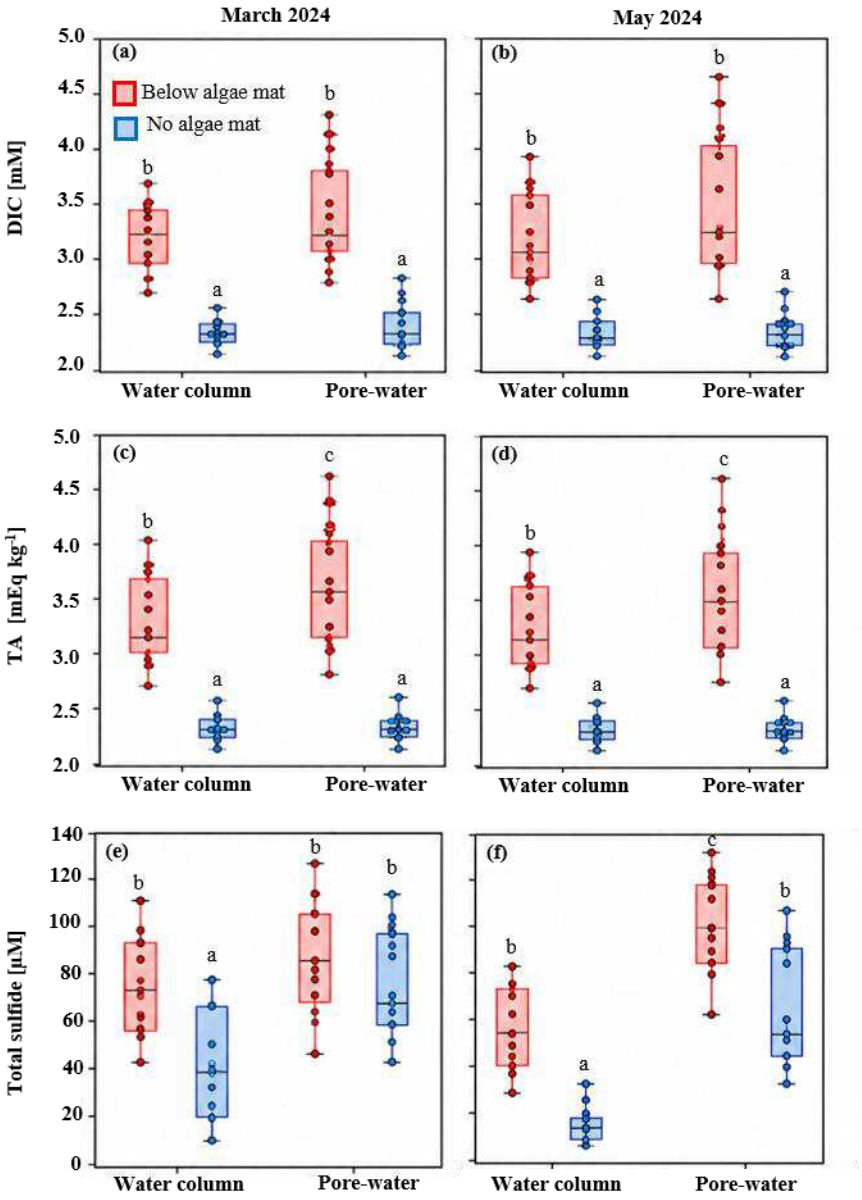

Fig. 4. *Porewater and water column chemistry at North Beach, Eilat, measured in March (bloom onset) and May (bloom senescence). Each panel shows four box groups: water column and porewater from algae-free seagrass (no mat, blue shades) and from beneath decomposing macroalgal mats (below mat, orange-red shades). Rows show DIC (a,b), TA (c,d), and total sulfide (e, f).*

3.3 Porewater geochemistry: sulfidic patch transects

Porewater DIC, TA, and total sulfide all increased sharply at the patch center relative to flanking seagrass sediment at both sampling timepoints, with the magnitude of

enrichment substantially greater during bloom senescence than at bloom onset (Fig. 5). Outside the patch, DIC and TA were similar between March and May, remaining within the range typical of seawater-equilibrated carbonate sediment porewater (~2.3 to 2.7 mM DIC; ~2.5 to 2.7 mM TA). Within the patch center (40 to 50 cm along the transect), both parameters increased sharply. In May, DIC reached values exceeding 10 mM and TA exceeded 9 mM, compared to peak values of approximately 2.9 mM DIC and 3.2 mM TA in March. The elevated TA tracked DIC closely at both timepoints, consistent with anaerobic remineralization as the dominant porewater modification process.

Dissolved sulfide was below detection outside the patch at both sampling times. Within the patch, sulfide peaked at approximately 0.21 mM in March and at approximately 2.1 mM in May, a tenfold increase between the two timepoints. Sulfide concentrations declined sharply within 10 to 15 cm of the patch center, returning to background levels at the flanking seagrass sediment. The spatial co-occurrence of elevated DIC, TA, and sulfide within the patch boundaries, and the close tracking of TA and DIC, are consistent with active biological sulfate reduction (BSR) fueled by decomposing macroalgal biomass.

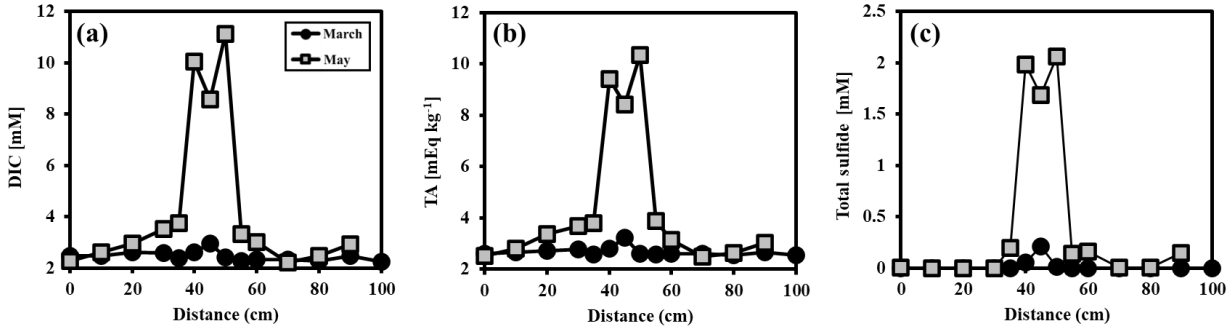

Fig. 5*. Porewater chemistry along a transect crossing a sulfidic patch in a H. stipulacea meadow at North Beach, Eilat, sampled at bloom onset (March 2024, blue circles) and bloom senescence (May 2024, red squares). (a) dissolved inorganic carbon, (b) total alkalinity, and (c) total dissolved sulfide, all in mM. The patch center is located at approximately 40–50 cm along the transect.*

3.4 Anaerobic decomposition slurry incubations

All organic matter treatments drove progressive anaerobic remineralization over the 25-day incubation, as indicated by coupled accumulation of alkalinity and sulfide and depletion of sulfate. The unamended sediment control showed no change in any measured parameter throughout the course of the experiment.

TA increased progressively in all organic matter treatments, rising from initial values of approximately 3 mEq kg-1 to 18 to 21 mEq kg-1 by day 25 (Fig. 6a). The rate of alkalinity increase was steepest in the leaves treatment during the first six days. Control incubations showed no alkalinity accumulation, confirming negligible anaerobic remineralization in unamended GoA sediment.

Total dissolved sulfide rose sharply within the first three days and remained elevated throughout the 25-day experiment in all organic matter treatments (Fig. 6b). Roots and rhizomes generated sulfide most rapidly, reaching approximately 0.7 mM by day 3 and exceeding 2.5 mM by day 9. Leaves followed a similar trajectory, with sulfide rising to approximately 0.6 mM by day 3 and plateauing between 2.0 and 2.5 mM from day 6 onward. The macroalgae treatment reached comparable concentrations more gradually, with a pronounced increase between days 3 and 9 (0.1 to 2.3 mM) and peak values approaching 3.0 mM at day 22. Control incubations produced no detectable sulfide at any timepoint, confirming negligible intrinsic sulfide-generating capacity in the unamended GoA sediment.

The three tissue fractions differed in their nutrient release dynamics. Leaves released ammonium rapidly, with blank-corrected NH_4^+ concentrations rising to approximately 40 µM by day 3, then declining and stabilizing between 10 and 20 µM for the remainder of the experiment (Fig. 6c). Roots and rhizomes and the macroalgae treatment showed minimal ammonium release throughout. Phosphate release was negligible in all treatments until approximately day 12 to 14, after which roots and rhizomes and leaves showed a gradual increase, reaching approximately 20 to 35 µM by day 25 (Fig. 6d). The macroalgae treatment showed a comparable phosphate increase only from day 20 onward. The control remained at or near zero for both nutrients.

Sulfate concentrations declined in parallel with sulfide accumulation in all organic matter treatments, decreasing by approximately 7 to 8 mM relative to an initial concentration of approximately 31.5 mM over the course of the experiment (Fig. 6e). The control remained stable at approximately 31 mM throughout, consistent with the absence of active sulfate reduction in unamended sediment.

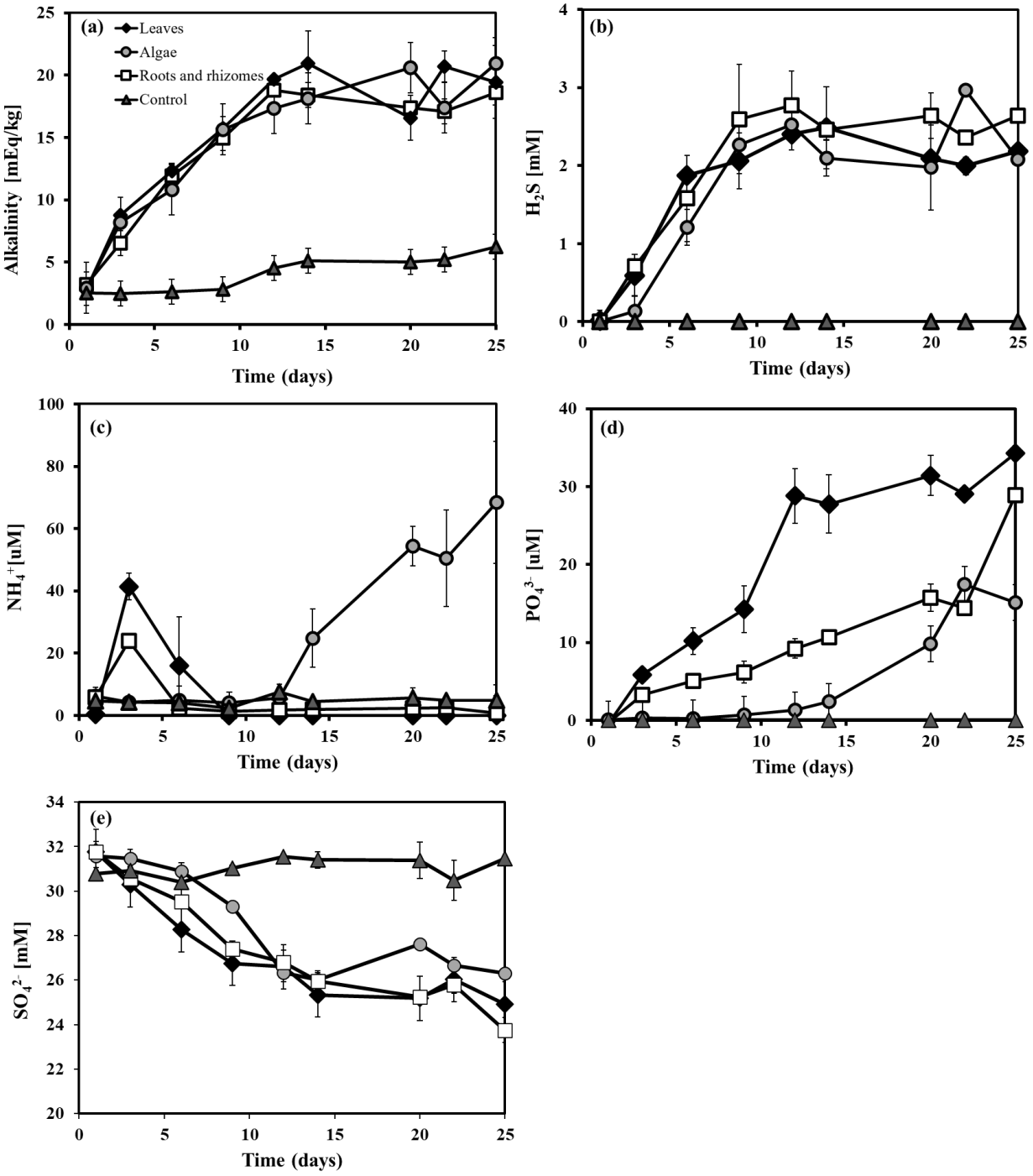

Fig. 6. *Time course of porewater chemistry during anaerobic decomposition of Halophila stipulacea tissue fractions and macroalgae in closed slurry incubations. (a) total alkalinity, (b) total dissolved sulfide, (c)ammonium, (d) phosphate, and (e) sulfate are shown over 25 days for four treatments: seagrass leaves (black diamonds), seagrass roots and rhizomes (white squares), algae (light gray dots), and an unamended sediment control (dark gray triangles).*

3.5 Mesocosm sulfide addition experiment

Net photosynthesis of *H. stipulacea* declined with increasing porewater sulfide concentration across a range spanning approximately four orders of magnitude (Fig. 7). At low sulfide concentrations (below approximately 10 µM), photosynthesis rates were highest, reaching values above 1.9 µmol O_2 h^{-1} cm^{-2}. Rates declined progressively with increasing sulfide, falling below 1 µmol O_2 h^{-1} cm^{-2} at concentrations above approximately 100 µM. Net photosynthesis became negative at the highest sulfide treatment (~3 mM), indicating that sulfide-driven respiratory inhibition exceeded gross photosynthetic oxygen production at that concentration.

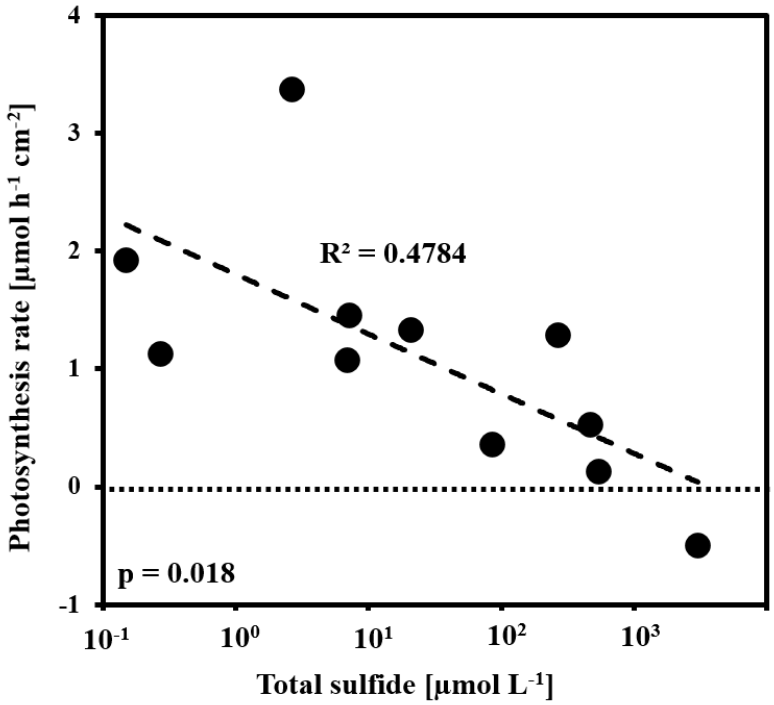

Fig. 7. *Photosynthesis rate (μmol O_2 h^{-1} cm^{-2}) of H. stipulacea as a function of porewater sulfide concentration (μM). The x-axis is plotted on a logarithmic scale. The dashed horizontal lineindicates zero net photosynthesis. The solid line represents linear regression fitted to log_{10}-transformed sulfide concentrations (R^2 = 0.48, p = 0.018, n = 11).*

4. Discussion

The field measurements and controlled experiments presented here document the biogeochemical cascade linking annual deep winter convective mixing in the GoA to physiologically consequential sulfide accumulation in *H. stipulacea* meadows. The cascade is established at the level of porewater chemistry and individual-shoot photosynthetic response. Here we first present the body of evidence supporting it and describe its mechanism in the context of the GoA with implications for porewater carbonate chemistry, climate forcing, and the broader typology of bloom-driven seagrass stress in oligotrophic systems.

4.1 Evidence for a bloom-driven sulfide cascade

Porewater TA, DIC, and total sulfide were elevated under decomposing mats relative to algae-free seagrass sediment at both sampling timepoints. All three signals intensified markedly between bloom onset in March and bloom senescence in May. Algae-free stations had porewater sulfide medians of 13 to 14 μM. These values fall well below the 50 to 500 μM range typical of healthy temperate seagrass beds [38] and establish the iron-buffered baseline of this oligotrophic carbonate system. By May, sulfide beneath mats had risen by more than an order of magnitude. TA and DIC reached values consistent with sustained anaerobic remineralization. The ΔTA:ΔDIC ratio approached the canonical 1:1 stoichiometry of net sulfate reduction ($CH_2O + SO_4^{2-} \rightarrow HCO_3^- + HS^- + H_2O$) [31]. This identifies BSR as the dominant remineralization pathway. Sulfide reoxidation would push it below unity [39], and carbonate dissolution would push it above. Therefore, the near-unity value observed therefore constrains both side reactions to a minor role within the bloom-affected sediment (Fig. 8). In the low-TA, low-DIC region of

the cross-plot (Fig. 8b), DIC increases with little corresponding rise in TA, likely due to aerobic respiration, which generates CO_2 with no alkalinity.

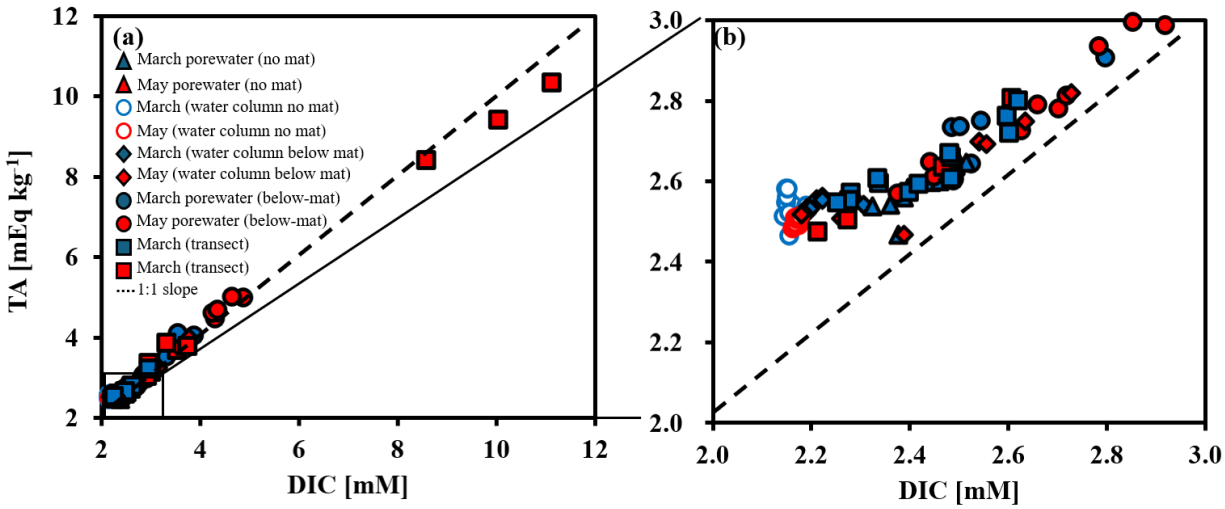

Fig. 8. DIC versus TA in porewater and overlying water collected at North Beach at a seagrass meadow covered by algae mat and meadow without algae. (a) Full data range; the black rectangle indicates the region expanded in panel (b). (b) Zoom view (2-6 mM) highlighting the baseline cluster. Blue symbols denote the March 2024 sampling (bloom onset); red symbols denote the May 2024 sampling (bloom senescence). Symbol types distinguish sample environments: stars, overlying water (OLW); open circles, porewater from algae-free seagrass stations (no-mat); filled circles, porewater from beneath macroalgal mats (below-mat); filled squares, sediment porewater along the sulfidic patch transect. The dashed line is the 1:1 reference.

The second line of evidence comes from the slurry experiments, which constrained the kinetics of the iron-buffer transition as both macroalgal and *H. stipulacea* tissue drove rapid sulfide accumulation in closed incubations (Fig. 6). The transition occurred once the most reactive Fe phases were consumed within the first three to five days [31]. Sulfate reduction proceeded effectively unbuffered thereafter, evident by the increase in total sulfide concentrations and decrease in sulfate concentrations (Fig. 6c). These experiments demonstrate mechanistically that labile organic matter loading can exhaust the GoA iron buffer on a timescale of days under closed conditions. They also show that

the macroalgal substrate is not categorically different from seagrass tissue in this respect. The contrast in the field reflects the magnitude and spatial concentration of macroalgal deposition rather than an intrinsic kinetic separation between substrates. The slurry results therefore generalize the field signal. Any sufficiently large pulse of labile organic carbon can overwhelm the buffer once contact between substrate and sediment is sustained over a period of days to weeks.

Two additional observations support but do not independently establish the cascade; Below-mat dissolved O_2 tracked the diel cycle in March with strong nocturnal drawdown to near-anoxia (Fig. 3). By May, O_2 was at or near zero throughout the 48-hour deployment and decoupled entirely from the overlying water column (Fig. 3b). The oxygen data are based on single deployments at each timepoint without replication and are therefore treated here as supporting rather than primary evidence. The localized sulfidic patch transect is similarly limited. Total sulfide reached approximately 2.1 mM at the patch center and declined sharply within 10 to 15 cm of the patch margin (Fig. 5c). This transect provides a spatial illustration of the heterogeneity expected from settled algal biomass infilling macrofaunal burrows. Yet, it is unreplicated and is not used to estimate aerial sulfide loading. It does, however, set a useful upper bound on locally observed concentrations during senescence and confirms that the cascade can produce strongly localized sulfidic microenvironments embedded within a more moderately enriched background.

The third line of evidence is the sulfide addition experiment. This experiment establishes the dose-response curve for *H. stipulacea* photosynthesis. No controlled sulfide exposure data previously existed for this species [23]. Photosynthetic suppression began above approximately 100 to 200 μM while net photosynthesis was effectively abolished at approximately 3 mM (Fig. 7). The threshold range falls below the porewater sulfide concentrations associated with documented seagrass die-off in Florida Bay and the Mediterranean [12, 17, 40-42]. It also lies well above the 0 to 14 μM background documented here for healthy GoA *H. stipulacea*. The field-measured below algae mat concentrations therefore fall within a physiologically consequential range. The dose-

response relationship provides the quantitative bridge between the sediment biogeochemistry and the plant physiology. Without it, the ecological significance of the porewater signal would remain unconstrained.

4.2 Mechanism in the Gulf of Aqaba context

The GoA cascade begins each winter with deep convective mixing. This process delivers nutrient-rich deep water into the photic zone of an otherwise oligotrophic basin [18]. Along the shallow coastal margin, the primary biological response to winter nutrient delivery is benthic macroalgal growth over the seagrass meadow. This reflects the basin's geometry: the GoA's narrow profile places shallow coastal habitats immediately adjacent to the open-sea convective column, so delivered nutrients reach the nearshore benthos before the pelagic community can assimilate them entirely. The result during the bloom period is a dense macroalgal mat overlying the meadow. Bloom magnitude scales with mixing depth, as deeper convection delivers proportionally greater nutrient loads to the photic zone. A purely pelagic response would deliver organic matter to the sediment more diffusely and over a longer timescale, reducing both the sulfide pulse and light attenuation to the sea floor.

Outside the bloom period, GoA sediments operate under a regulated, oxidized regime. Sulfide production is matched by reoxidation and Fe-mediated sequestration [21]. Aeolian deposition of reactive Fe(III) phases from Saharan dust sustains a cryptic sulfur cycle. The dust-derived Fe pool is dominated by hematite and goethite, with a smaller pool of more reactive ferrihydrite and lepidocrocite [37, 43]. BSR-derived sulfide is rapidly scavenged as iron sulfide. Direct quantification by Grijalva-Rodriguez et al. [21] showed that BSR rates in GoA shallow sediments are comparable to those in unaffected coastal sediments. Sulfide oxidation rate constants exceed those measured in iron-rich systems such as Svalbard fjords [44]. Steady-state porewater H_2S is held below 100 nM. The fine-to-medium carbonate sand at North Beach (63 to 250 μM) reinforces this buffered state as it allows oxygen to penetrate the upper sediment by advective and diffusive transport [42]. It also supports macrofaunal bioirrigation that continually regenerates Fe(III) at depth

[45]. This combination defines the buffered baseline against which the bloom-driven perturbation is set.

Macroalgal decomposition overwhelms this buffer through several reinforcing mechanisms. Labile macroalgal organic matter has C:N ratios of approximately 8 to 12, relative to 20 to 50 in seagrass tissue. This drives BSR at rates that substantially exceed those supported by seagrass detritus [17, 31, 45-47]. The kinetics are aggressive because sulfate-reducing bacteria are already present on living algal thalli and proliferate upon senescence [47]. Reactive Fe phases such as lepidocrocite and ferrihydrite are consumed first. The remaining buffer is then progressively depleted [42, 48]. A secondary mechanism likely amplifies this in the field: Senescent algal biomass settles into macrofaunal burrows (Fig. 1i). These burrows are normally the principal conduit for oxygen replenishment of the shallow subsurface through bioirrigation [49, 50]. Sealing of burrow openings by algal mat material would suppress bioturbation-driven Fe(III) regeneration. This compresses the iron buffer from both supply and demand sides simultaneously [51]. The net effect is a transition from a regulated to an unbuffered state on a timescale of weeks rather than months,

The intensification of stress from March to May requires explicit reconciliation with seagrass physiology. Population data from the Eilat coast show that *H. stipulacea* operates near its seasonal photosynthetic and structural minimum in late winter. Shoot density and aboveground biomass increase by approximately 35% and 18%, respectively, between February and the July maximum [27, 28]. Sparse canopies and low photosynthetic rates yield a contracted oxic rhizosphere at this time of year [12, 52-53]. The field data contradict this prediction. The resolution is that the dominant control on free sulfide in the GoA is organic matter supply and iron-buffer state rather than plant physiology. In March, the bloom had recently established and decomposition was in its initial stages. The iron buffer remained largely intact. By May, weeks of progressive decomposition had built a large standing stock of partially degraded, highly labile material in direct contact with sediment. Sustained BSR had progressively consumed reactive Fe phases [31, 42]. Temperature increase is an additional contributor. Water temperature in

the GoA increases by several degrees between March and May [54]. This translates to a two- to threefold increase in BSR rate for the same organic matter supply [55]. The system is therefore dominated by the supply side of the sulfide budget rather than by demand-side oxidative defenses that would otherwise track seagrass photosynthetic capacity.

The dose-response data place the field concentrations within a physiologically consequential range. The structural vulnerability of *H. stipulacea* deserves explicit treatment in this context. Holmer and Hasler-Sheetal (2014) [5] showed that *Zostera marina* precipitates elemental sulfur (S^0) on the inner walls of lacunar air spaces upon gaseous H_2S entry. This pathway accounts for up to 45% of net sulfur accumulation in plant tissue. Additional protection operates through enzymatic incorporation of sulfide into cysteine, glutathione, and other thiols. Both mechanisms depend on substantial aerenchymal volume and a long internal diffusion pathway *H. stipulacea* is structurally ill-suited to either requirement. Its leaves are typically less than 10 cm long. Its rhizomes are partially exposed at the sediment surface. Its belowground biomass is among the smallest of any seagrass studied [23, 26-27].

We did not quantify shoot density, areal cover, or mortality in this study. We therefore cannot evaluate directly whether the documented sulfide exposure translated into meadow-scale biomass loss. The cascade is established at the level of porewater chemistry and individual-shoot photosynthetic response. Whether annual sulfidic events produce transient patch-scale die-off followed by clonal recolonization, as has been observed in chronically loaded analogues [56], or whether the meadow absorbs the stress without measurable cover loss, is an open question. If die-off does occur, recovery is not guaranteed: positive feedbacks between meadow loss and sediment sulfide accumulation can sustain a degraded state even after the initial stressor subsides, as demonstrated for seagrass systems more broadly [57]. Recovery dynamics are similarly speculative on the basis of the present data. The architectural traits that limit *H. stipulacea*'s sulfide detoxification capacity also make it a rapid clonal colonizer [23, 26-27], but whether this translates into reoccupation of disturbed patches at the timescale relevant to annual bloom cycles cannot be evaluated here. Resolving these questions will

require monitoring studies designed around shoot density and patch dynamics on interannual timescales. The seasonal progression from bloom establishment through sulfidic stress to potential recovery is summarized in a conceptual model (Fig. 9).

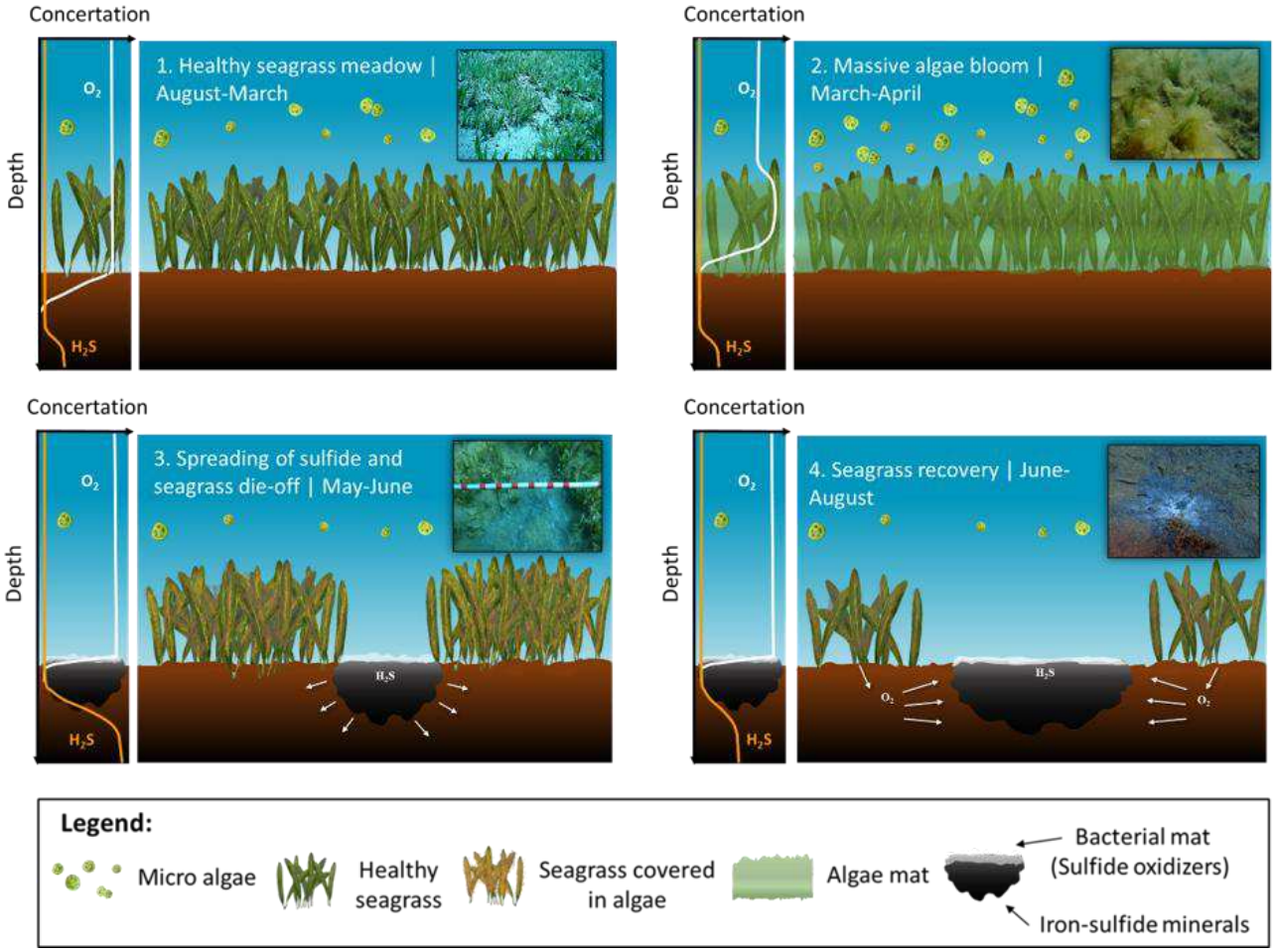

Fig. 9 *Conceptual model illustrating the seasonal progression of sulfide-driven seagrass decline and recovery following a massive algal bloom event. (1) During the healthy meadow stage (August–February), dense seagrass maintains oxidized sediment conditions through oxygen release from roots, restricting sulfide accumulation to deeper sediments. (2) A massive algal bloom develops during February–April, increasing organic matter deposition and sediment oxygen demand. (3) During May–June, enhanced sulfate reduction leads to sulfide accumulation and lateral spreading within the sediment, resulting in seagrass stress and die-off. Reduced root oxygenation further promotes sulfide expansion, creating a positive feedback between sulfide accumulation and meadow degradation. (4) During June–August, surviving seagrass patches begin to*

recover and reoxygenate surrounding sediments, limiting sulfide persistence and promoting recolonization. Insets show representative field photographs corresponding to each stage.

4.3 Implications

The GoA system documented here occupies a distinct position in the global typology of macroalgal mat-driven seagrass sulfide stress. Analogous cascades have been documented in Scandinavian *Zostera marina* meadows under experimentally deployed filamentous algal mats [52]. They have also been documented in Thau Lagoon under green algal degradation amplified by aquaculture organic loading [56], in Mediterranean *Posidonia oceanica* beds invaded by *Caulerpa* [58], and in the Yellow Sea where *Ulva prolifera* green tides generate acute benthic sulfidic conditions [22]. In all of these cases, the cascade is driven by chronic or seasonally sustained anthropogenic nutrient loading. The GoA differs fundamentally in the forcing mechanism. The bloom is generated by the basin's annual deep convective mixing cycle. This is a physically driven, naturally recurring nutrient pulse rather than continuous eutrophication. The episodic character of the forcing is the defining feature of the GoA cascade.

This episodic character has implications for recovery dynamics that we cannot test directly here. Under chronic loading, reactive iron pools become progressively and permanently depleted across successive seasons [59, 60]. Under episodic loading, iron reoxidation between annual mixing events and continuous aeolian Fe deposition [37, 42] may regenerate the reactive Fe pool before the next bloom cycle. Whether this regeneration is adequate is a testable hypothesis that we suggest but did not measure. The Yellow Sea *Ulva prolifera* analogue is informative on the controlling parameter. Guo et al. (2024) [22] showed that Fe-rich red soil additions effectively sequestered sulfide from *Ulva*-enriched sediments with minimal loss of buffering capacity over 18 days. The controlling parameter is the ratio of reactive Fe supply to labile organic carbon flux. In the GoA, this ratio is maintained in the buffered range across most of the year by aeolian dust deposition. It is challenged each spring by the bloom decomposition pulse. Whether the

system remains within the recoverable bound under future conditions is the central question for predicting its long-term trajectory.

Climate change introduces an additional layer of complexity. GoA surface temperatures have increased by 0.40 to 0.45°C per decade over recent decades [61]. The frequencyof complete water-column mixing events in the GoA has declined over the past two decades [62]. The net effect of these trends on bloom-driven sulfide stress is not straightforward. Less frequent or shallower deep mixing reduces nutrient entrainment. This should reduce average annual bloom biomass. Warmer sediment temperatures, in contrast, amplify BSR for any given organic matter input (e.g. [55]) Sulfide accumulation rates under decomposing macroalgal mats increase two- to threefold between 28 and 35°C [41, 63], meaning that a smaller bloom in warmer sediments may generate porewater sulfide concentrations equivalent to those produced by a larger bloom under cooler conditions. Reduced bloom biomass may therefore yield equivalent or greater sulfide accumulation under warmer conditions. The accelerating Mediterranean expansion of *H. stipulacea* into vacated *Cymodocea nodosa* and *Posidonia oceanica* habitat [64] suggests that the species' physiological breadth will favor it over native competitors under warming. This advantage does not extend to sulfide detoxification. Structural constraints set the limit. The net trajectory of sulfidic patch formation frequency and severity in GoA seagrass meadows under continued warming cannot be predicted from any single forcing alone.

The cascade also has direct consequences for porewater carbonate chemistry. The sustained alkalinity generation observed under mats reached TA values of 9 mEq kg^{-1} at the patch center. This represents a CO_2 removal pathway that operates in parallel with seagrass primary production. The alkalinity signal propagates into the overlying water column over time. Partial coupling between porewater and water-column TA was observed in May, consistent with this propagation. The same biogeochemical cascade that stresses the seagrass therefore generates a measurable alkalinity flux to bottom waters. The implications for net coastal CO_2 exchange warrant separate quantification. The result is a coupling between sulfide-driven seagrass stress and basin-scale carbonate chemistry that is not accounted for in current oligotrophic seagrass carbon

budgets. Whether the alkalinity flux partially offsets the carbon-sequestration penalty associated with sulfide-driven seagrass impairment is an open question. It is one that depends on the relative magnitudes of stress-induced productivity loss and BSR-driven alkalinity export.

Beyond the GoA, these results extend the documented macroalgal mat-driven seagrass sulfide stress from chronically eutrophied systems into naturally oligotrophic basins. The forcing in suchsystems is physical and episodic rather than anthropogenic and chronic. Mediterranean and Red Sea oligotrophic basins host extensive seagrass meadows on carbonate or carbonate-influenced substrates. Iron buffering may be particularly limited in these settings [65]. Mechanisms that operate independently of nutrient pollution identify natural variability as an underappreciated control on seagrass ecosystem function in oligotrophic systems. The implications extend to the global seagrass carbon sink. Seagrass meadows account for a disproportionate share of marine carbon burial despite covering less than 0.2% of the seafloor [1, 2]. Mechanisms of meadow stress that are decoupled from nutrient pollution therefore deserve explicit consideration alongside eutrophication in projections of global seagrass carbon dynamics.

5. Conclusions

Annual deep winter convective mixing in the GoA generates a biogeochemical cascade that produces physiologically consequential sulfidic stress in *H. stipulacea* meadows. Decomposing macroalgal biomass drives biological sulfate reduction that overwhelms the sediment iron buffer, elevating porewater sulfide beneath mats by more than an order of magnitude between bloom onset in March and senescence in May. Controlled sulfide exposures establish, for the first time, a dose-response relationship for photosynthetic suppression in this species, and the field-measured concentrations beneath mats fall within the range that suppresses net photosynthesis. The same cascade generates substantial alkalinity fluxes to bottom waters, coupling sulfide-driven seagrass stress to basin-scale carbonate chemistry in a way not currently accounted for in oligotrophic seagrass carbon budgets. Together, these results provide the first quantitative porewater

sulfide baseline for healthy *H. stipulacea* meadows in the GoA and a mechanistic link between a naturally recurring physical forcing and sulfidic seagrass stress in an oligotrophic, iron-buffered carbonate system.

Whether this stress translates to measurable meadow-scale biomass loss remains unresolved. The structural traits that limit *H. stipulacea*'s sulfide detoxification capacity also make it a rapid clonal colonizer, but whether recolonization keeps pace with annual sulfidic disturbance cannot be evaluated from the present data. The broader significance of these results lies in their decoupling of bloom-driven sulfide stress from anthropogenic nutrient loading. Physical forcing alone issufficient to produce it. Eutrophication pressure is expected to amplify the magnitude of these events, as additional nutrient loading would sustain larger macroalgal biomass and prolong the decomposition pulse beyond what physical forcing alone delivers. Whether aeolian iron deposition regenerates the GoA sediment buffer between successive bloom cycles, and whether warming-driven changes in mixing depth alter the balance between organic matter supply and iron-buffer capacity, are the central questions for predicting the long-term trajectory of these meadows.

Author contributions

Neta Soto: Investigation, Formal analysis, Visualization, Writing – original draft, Writing – review & editing. Maayan Mazal Malul: Investigation, Writing – review & editing. Gilad Antler: Conceptualization, Methodology, Formal analysis, Investigation, Resources, Data curation, Visualization, Supervision, Project administration, Funding acquisition.

Ethics statement

Field collection of *Halophila stipulacea* and *Ulva lactuca* specimens was conducted under permit number 2023/43223 issued by the Israel Nature and Parks Authority. No human subjects, human data, or vertebrate animals were involved in this study.

Funding statement

This work was supported by the Israel Science Foundation (grant no. 2010/24 to G.A.) and the United States-Israel Binational Science Foundation (grant no. 2024291).

Data availability statement

The datasets generated during this study are available as supplementary material accompanying this article, including porewater geochemistry (total dissolved sulfide, total alkalinity, dissolved inorganic carbon) from field sampling at bloom onset and senescence, dissolved oxygen time series from optode deployments, geochemical data from the anaerobic slurry decomposition incubations, and porewater sulfide and photosynthesis rate data from the mesocosm sulfide addition experiment.

Competing interests

The authors declare no competing interests.

References

[1] Duarte, C. M., Middelburg, J. J., & Caraco, N. (2005). Major role of marine vegetation on the oceanic carbon cycle. Biogeosciences, 2(1), 1–8. https://doi.org/10.5194/bg-2-1-2005

[2] Fourqurean, J. W., Duarte, C. M., Kennedy, H., Marbà, N., Holmer, M., Mateo, M. A., Apostolaki, E. T., Kendrick, G. A., Krause-Jensen, D., McGlathery, K. J., & Serrano, O. (2012). Seagrass ecosystems as a globally significant carbon stock. Nature Geoscience, 5(7), 505–509. https://doi.org/10.1038/ngeo1477

[3] Waycott, M., Duarte, C. M., Carruthers, T. J. B., Orth, R. J., Dennison, W. C., Olyarnik, S., Calladine, A., Fourqurean, J. W., Heck, K. L., Jr., Hughes, A. R., Kendrick, G. A., Kenworthy, W. J., Short, F. T., & Williams, S. L. (2009). Accelerating loss of seagrasses across the globe threatens coastal ecosystems. *Proceedings of the National Academy of Sciences*, *106*(30), 12377–12381. https://doi.org/10.1073/pnas.0905620106

[4] Lamers, L. P. M., Govers, L. L., Janssen, I. C. J. M., Geurts, J. J. M., Van der Welle, M. E. W., Van Katwijk, M. M., Van der Heide, T., Roelofs, J. G. M., & Smolders, A. J. P. (2013). Sulfide as a soil phytotoxin: A review. Frontiers in Plant Science, 4, 268. https://doi.org/10.3389/fpls.2013.00268

[5] Holmer, M., & Hasler-Sheetal, H. (2014). Sulfide intrusion in seagrasses assessed by stable sulfur isotopes, a synthesis of current results. Frontiers in Marine Science, 1, 64. https://doi.org/10.3389/fmars.2014.00064

[6] Hasler-Sheetal, H., & Holmer, M. (2015). Sulfide intrusion and detoxification in the seagrass Zostera marina. PLOS ONE, 10(6), e0129136. https://doi.org/10.1371/journal.pone.0129136

[7] Larkum, A. W. D., Kendrick, G. A., & Ralph, P. J. (Eds.). (2018) Seagrasses of Australia: Structure, ecology and conservation. Springer

[8] Fraser, M. W., Martin, B. C., Wong, H. L., Burns, B. P., & Kendrick, G. A. (2023). Sulfide intrusion in a habitat forming seagrass can be predicted from relative abundance of sulfur cycling genes in sedimentsScience of the Total Environment ,864, 161144. https://doi.org/10.1016/j.scitotenv.2022.161144

[9] Martin, B. C., & Maricle, B. R. (2015). Species-specific enzymatic tolerance of sulfide toxicity in plant roots. Plant Physiology and Biochemistry, 88, 36–41. https://doi.org/10.1016/j.plaphy.2015.01.007

[10] Raven, J. A., & Scrimgeour, C. M. (1997). The influence of anoxia on plants of saline habitats with special reference to the sulphur cycle Annals of Botany, 79 (Supplement A), 79–86. https://doi.org/10.1093/oxfordjournals.aob.a010309

[11] Martin, B. C., Bougoure, J., Ryan, M. H., Bennett, W. W., Colmer, T. D., Joyce, N. K., Olsen, Y. S., & Kendrick, G. A. (2019). Oxygen loss from seagrass roots coincides

with colonisation of sulphide-oxidising cable bacteria and reduces sulphide stress. *The ISME Journal*, *13*(3), 707–719. https://doi.org/10.1038/s41396-018-0308-5

[12] Borum, J., Pedersen, O., Greve, T. M., Frankovich, T. A., Zieman, J. C., Fourqurean, J. W., & Madden, C. J. (2005). The potential role of plant oxygen and sulphide dynamics in die-off events of the tropical seagrass, Thalassia testudinum. Journal of Ecology, 93(1), 148–158. https://doi.org/10.1111/j.1365-2745.2004.00943

[13] Winn, N. H., Koch, M. S., & Madden, C. J. (2025). Lack of root oxygen loss from the dominant tropical Atlantic-Caribbean seagrass,Thalassia testudinum, in a highly sulfidic carbonate lagoonJournal of Experimental Marine Biology and Ecology,589, 152113. https://doi.org/10.1016/j.jembe.2025.152113

[14] Lindell, D., & Post, A. F. (1995). Ultraphytoplankton succession is triggered by deep winter mixing in the Gulf of Aqaba (Eilat), Red Sea. Limnology and Oceanography, 40(6), 1130–1141. https://doi.org/10.4319/lo.1995.40.6.1130

[15] Labiosa, R. G., Arrigo, K. R., Genin, A., Monismith, S. G., & van Dijken, G. (2003). The interplay between upwelling and deep convective mixing in determining the seasonal phytoplankton dynamics in the Gulf of Aqaba: Evidence from SeaWiFS and MODIS. Limnology and Oceanography, 48(6), 2355–2368. https://doi.org/10.4319/lo.2003.48.6.2355

[16] Avrahami, Y., Koplovitz, G., & Frada, M. J. (2025). Diatom community succession and bloom variability as a function of winter-mixing depth in the subtropical Gulf of Aqaba, Red Sea. Marine Ecology Progress Series, 760, 39–54. https://doi.org/10.3354/meps14848

[17] Carlson, P. R., Yarbro, L. A., & Barber, T. R. (1994). Relationship of sediment sulfide to mortality of Thalassia testudinum in Florida Bay. Bulletin of Marine Science, 54(3), 733–746

[18] Genin, A., Lazar, B., & Brenner, S. (1995). Vertical mixing and coral death in the Red Sea following the eruption of Mount Pinatubo. Nature, 377(6549), 507–510. https://doi.org/10.1038/377507a0

[19] Zarubin, M., Lindemann, Y., & Genin, A. (2017). The Dispersion-Confinement mechanism of phytoplankton blooms in a two-layer sea. Progress in Oceanography, 155, 13–27. https://doi.org/10.1016/j.pocean.2017.05.005

[20] Shaked, Y., & Fine, M. (2025). The Israel National Monitoring Program in the Northern Gulf of Aqaba: Scientific report 2025. Israel Ministry of Environmental Protection

[21] Grijalva-Rodriguez, T. I., Antler, G., Eliani-Russak, E., Feng, D., Gong, S., Pellerin, A., Røy, H., Solomovich, K., Turchyn, A. V., Zweig, I., & Kamyshny, A., Jr. (2026). Sulfate reduction and hydrogen sulfide oxidation rates in marine sediments with cryptic sulfur cycling. Journal of the Geological Society, 183. https://doi.org/10.1144/jgs2025-088

[22] Guo, Y. Y., Li, T., Cao, X. Y., & Zhu, M. X. (2024). Effective capping of dissolved sulfide generated in Ulva prolifera-rich marine sediments by iron-rich red soil. Marine Pollution Bulletin, 203, 116424. https://doi.org/10.1016/j.marpolbul.2024.116424

[23] Winters, G., Beer, S., Willette, D. A., Viana, I. G., Chiquillo, K. L., Beca-Carretero, P., Villamayor, B., Azcárate-García, T., Shem-Tov, R., Mwabvu, B., Migliore, L., Rotini, A., Oscar, M. A., Belmaker, J., Gamliel, I., Alexandre, A., Engelen, A. H., Procaccini, G., & Rilov, G. (2020). The tropical seagrass Halophila stipulacea: Reviewing what we know from its native and invasive habitats, alongside identifying knowledge gaps. Frontiers in Marine Science, 7, 300. https://doi.org/10.3389/fmars.2020.00300

[24] Sharon, Y., Levitan, O., Spungin, D., Berman-Frank, I., & Beer, S. (2011). Photoacclimation of the seagrass Halophila stipulacea to the dim irradiance at its 48-

meter depth limit. Limnology and Oceanography, 56(1), 357–362 https://doi.org/10.4319/lo.2011.56.1.0357

[25] Winters, G., Edelist, D., Shem-Tov, R., Beer, S., & Rilov, G. (2017). A low cost field-survey method for mapping seagrasses and their potential threats: An example from the northern Gulf of Aqaba, Red Sea. Aquatic Conservation: Marine and Freshwater Ecosystems, 27(2), 324–339. https://doi.org/10.1002/aqc.2688

[26] Azcárate-García, T., Beca-Carretero, P., Villamayor, B., Stengel, D. B., & Winters, G. (2020). Responses of the seagrass Halophila stipulacea to depth and spatial gradients in its native region (Red Sea): Morphology, in situ growth and biomass production. Aquatic Botany, 165, 103242. https://doi.org/10.1016/j.aquabot.2020.103252

[27] Beca-Carretero, P., Rotini, A., Mejia, A., Migliore, L., Vizzini, S., & Winters, G. (2020). Halophila stipulacea descriptors in the native area (Red Sea): A baseline for future comparisonswith native and non-native populations. Marine Environmental Research, 153, 104828. https://doi.org/10.1016/j.marenvres.2019.104828

[28] Nguyen, H. M., Savva, I., Kleitou, P., Kletou, D., Lima, F. P., Sapir, Y., & Winters, G. (2020). Seasonal dynamics of native and invasive Halophila stipulacea populations: A case study from the northern Gulf of Aqaba and the eastern Mediterranean Sea. Aquatic Botany, 162, 103205. https://doi.org/10.1016/j.aquabot.2020.10320

[29] Apostolaki, E. T., Holmer, M., Marbà, N., & Karakassis, I. (2018). Sulfide intrusion in seagrasses from the Eastern Mediterranean Sea. Marine Environmental Research, 134, 85–95. https://doi.org/10.1016/j.marenvres.2017.12.006

[30] Dutta, S., Saar, R., Lavie, Z., Vered, G., Bradbury, H. J., & Antler, G. (2022). A method for a fast and economical in situ collection of pore water in sandy sediments. Frontiers in Marine Science, 9, 968063. https://doi.org/10.3389/fmars.2022.968063

[31] Soto, N., Winters, G., & Antler, G. (2023). The biogeochemical fingerprints of Halophila stipulacea decomposition in marine sediments of the Gulf of Aqaba. Frontiers in Marine Science, 10, 1250931. https://doi.org/10.3389/fmars.2023.1250931

[32] Mejia, A. Y., Rotini, A., Lacasella, F., Bookman, R., Thaller, M. C., Shem-Tov, R., Winters, G., & Migliore, L. (2016). Assessing the ecological status of seagrasses using morphology, biochemistry, and microbial community in the northern Red Sea. Marine Pollution Bulletin, 109(1), 552–562. https://doi.org/10.1016/j.ecolind.2015.09.014

[33] Dickson, A. G., Sabine, C. L., & Christian, J. R. (Eds.). (2007). Guide to best practices for ocean CO_2 measurements (PICES Special Publication 3). North Pacific Marine Science Organization. https://doi.org/10.25607/OBP-1342

[34] Cline, J. D. (1969). Spectrophotometric determination of hydrogen sulfide in natural waters. Limnology and Oceanography, 14(3), 454–458. https://doi.org/10.4319/lo.1969.14.3.0454

[35] Nagul, E. A., McKelvie, I. D., Worsfold, P., & Kolev, S. D. (2015). The molybdenum blue reaction for the determination of orthophosphate revisited: Opening the black box. Analytica Chimica Acta, 890, 60–82. https://doi.org/10.1016/j.aca.2015.07.030

[36] Stookey, L. L. (1970). Ferrozine: A new spectrophotometric reagent for iron. Analytical Chemistry, 42(7), 779–781. https://doi.org/10.1021/ac60289a016

[37] Blonder, B., Boyko, V., Turchyn, A. V., Antler, G., Sinichkin, U., Knossow, N., Klein, R., & Kamyshny, A. (2017). Impact of aeolian dry deposition of reactive iron minerals on sulfur cycling in sediments of the Gulf of Aqaba. Frontiers in Microbiology, 8, 1131. https://doi.org/10.3389/fmicb.2017.01131

[38] Terrados, J., Duarte, C. M., Kamp-Nielsen, L., Agawin, N. S. R., Gacia, E., Lacap, D., Fortes, M. D., Borum, J., Lubanski, M., & Greve, T. (1999). Are seagrass growth and

survival constrained by the reducing conditions of the sediment? Aquatic Botany, 65(1–4), 175–197. https://doi.org/10.1016/S0304-3770(99)00039-X

[39] Soetaert, K., Hofmann, A. F., Middelburg, J. J., Meysman, F. J. R., & Greenwood, J. (2007). The effect of biogeochemical processes on pH. Marine Chemistry, 105(1–2), 30–51. https://doi.org/10.1016/j.marchem.2006.12.012.

[40] Hall, M. O., Furman, B. T., Merello, M., & Durako, M. J. (2016). Recurrence of Thalassia testudinum seagrass die-off in Florida Bay, USA: Initial observations. Marine Ecology Progress Series, 560, 243–249. https://doi.org/10.3354/meps11923

[41] Calleja, M. Ll., Marbà, N., & Duarte, C. M. (2007). The relationship between seagrass (Posidonia oceanica) decline and sulfide porewater concentration in carbonate sediments. Estuarine, Coastal and Shelf Science, 73, 583–588. https://doi.org/10.1016/j.ecss.2007.02.016

[42] Koch, M. S., Schopmeyer, S. A., Kyhn-Hansen, C., & Madden, C. J. (2007). Synergistic effects of high temperature and sulfide on tropical seagrass. Journal of Experimental Marine Biology and Ecology, 341(1), 91–101. https://doi.org/10.1016/j.jembe.2006.10.004

[43] Boyko, V., Blonder, B., & Kamyshny, A. (2019). Sources and transformations of iron in the sediments of the Gulf of Aqaba (Red Sea). Marine Chemistry, 216, 103691. https://doi.org/10.1016/j.marchem.2019.103691

[44] Michaud, A. B., Laufer, K., Findlay, A., Pellerin, A., Antler, G., Turchyn, A. V., Warembourg, C., Røy, H., & Jørgensen, B. B. (2020). Glacial influence on the iron and sulfur cycles in Arctic fjord sediments (Svalbard). *Geochimica et Cosmochimica Acta*, 280, 423–440. https://doi.org/10.1016/j.gca.2019.12.033

[45] Antler, G., Mills, J. V., Hutchings, A. M., Redeker, K. R., & Turchyn, A. V. (2019). The sedimentary carbon-sulfur-iron interplay–A lesson from East Anglian salt marsh sediments. Frontiers in Earth Science, 7, 140. https://doi.org/10.3389/feart.2019.00140

[46] Kristensen, E. (1994). Decomposition of macroalgae, vascular plants and sediment detritus in seawater: Use of stepwise thermogravimetry. Biogeochemistry, 26(1), 1–24. https://doi.org/10.1007/BF02180401

[47] Nedergaard, R. I., Risgaard-Petersen, N., & Finster, K. (2002). The importance of sulfate reduction associated with Ulva lactuca thalli during decomposition: A mesocosm experiment. Journal of Experimental Marine Biology and Ecology, 275(1), 15–29. https://doi.org/10.1016/S0022-0981(02)00211-3

[48] Canfield, D. E. (1989). Reactive iron in marine sediments. Geochimica et Cosmochimica Acta, 53(3), 619–632. https://doi.org/10.1016/0016-7037(89)90005-7

[49] Bialik, O.M., Bookman, R., Elyashiv, H., Marietou, A., Saar, R., Rivlin, T., Taha, N., Benaltabet, T., Lotem, N., Funaro, E. and Antler, G., 2022. Tropical storm-induced disturbance of deep-water porewater profiles, Gulf of Aqaba. Marine Geology, 453, p.106926. https://doi.org/10.1016/j.margeo.2022.106926

[50] Boyko, V., Torfstein, A., & Kamyshny, A. (2018). Oxygen consumption in permeable and cohesive sediments of the Gulf of Aqaba. Aquatic Geochemistry, 24(3), 165–193. https://doi.org/10.1007/s10498-018-9338-x

[51] van de Velde, S. J., Hidalgo-Martinez, S., Callebaut, I., Antler, G., James, R. K., Leermakers, M., & Meysman, F. J. (2020). Burrowing fauna mediate alternative stable states in the redox cycling of salt marsh sediments. Geochimica et Cosmochimica Acta, 276, 31-49. https://doi.org/10.1016/j.gca.2020.02.021

[52] Holmer, M., & Nielsen, R. M. (2007). Effects of filamentous algal mats on sulfide invasion in eelgrass (Zostera marina). Journal of Experimental Marine Biology and Ecology, 353(2), 245–252. https://doi.org/10.1016/j.jembe.2007.09.010

[53] Brodersen, K. E., Koren, K., Moßhammer, M., Ralph, P. J., Kühl, M., & Santner, J. (2017). Seagrass-mediated phosphorus and iron solubilization in tropical sediments. Environmental science & technology, 51(24), 14155-14163.. https://doi.org/10.1021/acs.est.7b03878

[54] Abir, S., McGowan, H. A., Shaked, Y., Gildor, H., Morin, E., & Lensky, N. G. (2024). Air–sea interactions in stable atmospheric conditions: lessons from the desert semi-enclosed Gulf of Eilat (Aqaba)Atmospheric Chemistry and Physics,24, 6177–6195. https://doi.org/10.5194/acp-24-6177-2024

[55] Robador, A., Brüchert, V., Steen, A. D., & Arnosti, C. (2010). Temperature induced decoupling of enzymatic hydrolysis and carbon remineralization in long-term incubations of Arctic and temperate sedimentsGeochimica et Cosmochimica Acta,74(8), 2316-2326. https://doi.org/10.1016/j.gca.2010.01.022

[56] Plus, M., Deslous-Paoli, J.-M., & Dagault, F. (2003). Seagrass (Zostera marina L.) bed recolonisation after anoxia-induced full mortality. Aquatic Botany, 77(2), 121–134. https://doi.org/10.1016/S0304-3770(03)00089-5

[57] van der Heide, T., van Nes, E. H., Geerling, G. W., Smolders, A. J. P., Bouma, T. J., & van Katwijk, M. M. (2007). Positive feedbacks in seagrass ecosystems: Implications for success in conservation and restoration. Ecosystems, 10(8), 1311–1322. https://doi.org/10.1007/s10021-007-9099-7

[58] Holmer, M., Marbà, N., Lamote, M., & Duarte, C. M. (2009). Deterioration of sediment quality in seagrass meadows (Posidonia oceanica) invaded by macroalgae (Caulerpa sp.). Estuaries and Coasts, 32(3), 456–466.

https://doi.org/10.1007/s12237-009-9133-4

[59] Haviland, K. A., Howarth, R. W., Marino, R., & Hayn, M. (2022). Variation in sediment and seagrass characteristics reflect multiple stressors along a nitrogen-enrichment gradient in a New England lagoon. Limnology and Oceanography, 67(3), 660–672. https://doi.org/10.1002/lno.12025

[60] Haviland, K. A., Howarth, R. W., Giblin, A. E., & Marino, R. (2024). The potential role of sediment iron and sulfur speciation in seagrass meadow loss and recovery. Ocean-Land-Atmosphere Research, 3, 0069. https://doi.org/10.34133/olar.0069

[61] Chaidez, V., Dreano, D., Agusti, S., Duarte, C. M., & Hoteit, I. (2017). Decadal trends in Red Sea maximum surface temperature. Scientific Reports, 7, 8144. https://doi.org/10.1038/s41598-017-08146-z

[62] Sengupta, S., Gildor, H., & Ashkenazy, Y. (2024). Depth-dependent warming of the Gulf of Eilat (Aqaba). Climatic Change, 177(7), 107. https://doi.org/10.1007/s10584-024-03765-8

[63] Höffle, H., Thomsen, M. S., & Holmer, M. (2011). High mortality of Zostera marina under high temperature regimes but minor effects of the invasive macroalgae Gracilaria vermiculophylla. Estuarine, Coastal and Shelf Science, 92(1), 35–46. https://doi.org/10.1016/j.ecss.2010.12.017

[64] Winters, G., Nguyen, H. M., & Kaminer, M. (2024). Expansion of Halophila stipulacea in parallel with declines of native seagrasses in the eastern Mediterranean Sea. Aquatic Botany, 194, 103781. https://doi.org/10.1016/j.aquabot.2024.103829

[65] Marbà, N., Calleja, M. L., Duarte, C. M., Álvarez, E., Díaz-Almela, E., & Holmer, M. (2007). Iron additions reduce sulfide intrusion and reverse seagrass (Posidonia oceanica)

decline in carbonate sediments. Ecosystems, 10(5), 745–756. https://doi.org/10.1007/s10021-007-9053-8

Supplementary Files

This is a list of supplementary files associated with this preprint. Click to download.

- SOISotoetal.xlsx